PRACTICAL SUPERCONDUCTOR DEVELOPMENT FOR ELECTRICAL POWER APPLICATIONS ARGONNE NATIONAL LABORATORY QUARTERLY REPORT FOR THE PERIOD ENDING MARCH 31, 2004

This is a multiyear experimental research program that focuses on improving relevant material properties of high-critical-temperature (T_c) superconductors and developing fabrication methods that can be transferred to industry for production of commercial conductors. The development of teaming relationships through agreements with industrial partners is a key element of the Argonne National Laboratory (ANL) program.

Technical Highlights

Several findings are highlighted. First, Raman spectroscopy shows that the removal of silver from YBCO using ammoniacal peroxide changes the film's microstructure more significantly than previously believed. To accurately characterize YBCO conductors by Raman spectroscopy, the YBCO film should be analyzed before it is coated with silver. Second, we correlate the tilt of YBCO grains and their Raman spectra so that Raman spectroscopy can be used to measure the tilt of YBCO in conductors made by inclined substrate deposition (ISD). Third, we compare the crystallographic and superconducting properties of $SrRuO_3$-buffered ISD/YBCO conductors that were fabricated with ISD deposition angle, α, of 35° or 55°. Transport measurements at 77 K indicated a critical current density, J_c, of 0.77×10^6 A/cm^2 for a sample made with α=35°.

YBCO Surface Modifications Caused by Removal of Silver Coating

Raman spectroscopy of YBCO films is ideally done before the film is covered with a thin (≈2 μm) layer of silver that is applied to protect the superconductor from atmospheric contamination and to ensure low contact resistance during the measurement of transport critical current. If a silver coating has already been applied, however, it has been considered acceptable to analyze the YBCO after ammoniacal peroxide is used to remove the silver. When the silver was dissolved in this way, the rinse solution tended to remove impurities from the YBCO surface in addition to the silver. It was also noticed that the intensity of the O(4) YBCO phonon (at 500 cm^{-1}) diminished in the spectrum of the rinsed film. This decrease in intensity was attributed to the

simultaneous removal of surface YBCO grains that formed with tilted c-axes as they grew around barium cuprate precipitates. In this report, we show that YBCO films rinsed with ammoniacal peroxide are changed more profoundly than previously believed and that the Raman spectra of such YBCO films are not representative of the microstructure of the as-deposited film.

For this investigation, we used a YBCO film deposited by pulsed laser deposition (PLD) on CeO_2/YSZ/MgO(100), in which the CeO_2 and yttria-stabilized zirconia (YSZ) layers were deposited by PLD on a (100)-oriented MgO single crystal. Raman spectra were collected from the film before it was coated with silver and after the silver was etched away. Representative spectra are shown in Fig. 1.

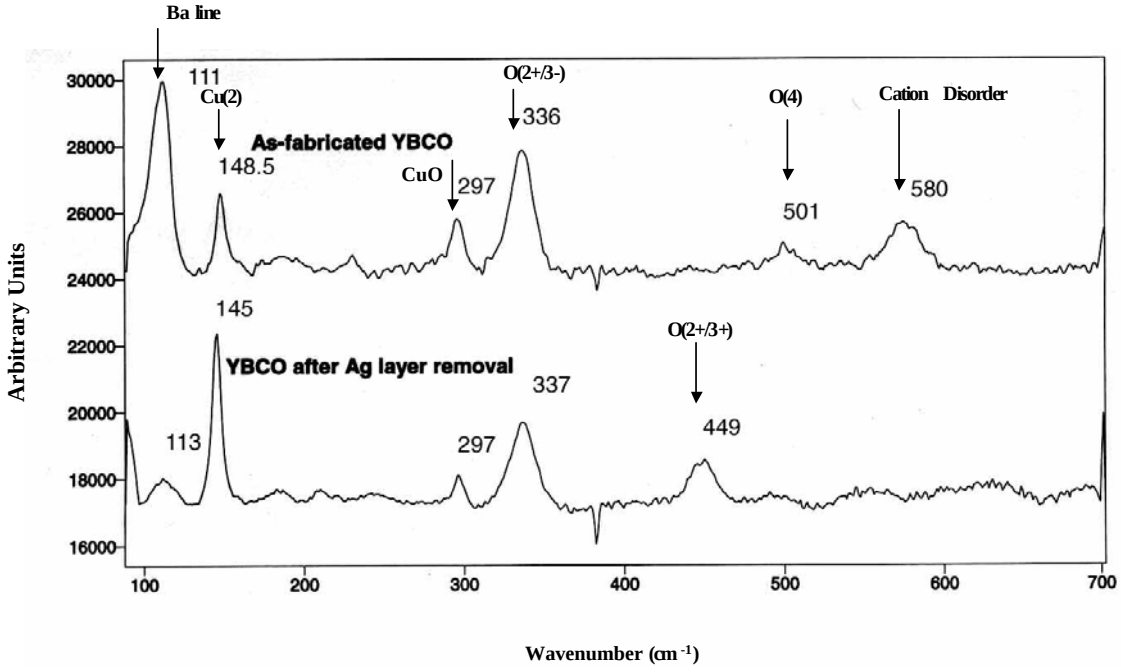

Fig. 1. Raman spectra of YBCO film before being coated with Ag and after Ag coating was removed by ammoniacal peroxide rinse.

The Raman spectrum of the as-produced YBCO film revealed that it consisted mainly of orthorhombic domains with an oxygen stoichiometry close to seven, as indicated by the occurrence of Cu(2) and O(4) phonons at 148 and 501 cm^{-1}, respectively. Because the spectrum showed faint evidence of the O(4) mode in addition to the O(2+/3-) phonon (336 cm^{-1}), we concluded that a small fraction of the YBCO grains was c-axis tilted and/or a-axis oriented. The

spectrum also showed that the film contained CuO (297 cm^{-1}) and cation disorder that was probably associated with second-phase formation (≈580 cm^{-1}).

After the silver was dissolved from the YBCO film, the peak at ≈580 cm^{-1} disappeared almost totally. The intensity of the O(4) mode (495-501 cm^{-1}) also decreased, which indicated that second-phase precipitates and some a-axis oriented grains had been removed from the surface. Also, the positions of the O(4) and Cu(2) phonons shifted to lower values (from 501 to 495 and from 148 to 145 cm^{-1}, respectively), indicating a depletion of oxygen from the top YBCO layers. Moreover, a new peak associated with the O(2+/3+) phonon of tetragonal YBCO emerged at 450 cm^{-1}. In addition, the intensity of the Ba line at 113 cm^{-1} decreased significantly, which also evidences the presence of tetragonal YBCO domains [1].

These results show that using an ammoniacal peroxide rinse to remove silver from a YBCO film significantly changes the YBCO. Impurity phases and tilted YBCO grains in their vicinity are dislodged along with the silver, and the top layers of YBCO appear to lose oxygen. Therefore, accurate characterization of YBCO conductors by Raman spectroscopy requires that the YBCO film be analyzed before it is coated with silver.

Determination of ISD-Induced YBCO Tilt by Raman Analysis

We describe here a recently discovered correlation between the tilt of YBCO grains and specific features of the film's Raman spectrum. YBCO films for this study were deposited on templates made by the ISD method with the architecture SRO/HE-MgO/ISD-MgO/YSZ/HC. In this structure, HC is the Hastelloy C substrate, YSZ is yttria-stabilized zirconia, ISD-MgO is the template layer made by the ISD method, HE-MgO is a homoepitaxial layer that sharpens the texture and reduces the roughness of the template layer, and SRO is $SrRuO_3$, which further sharpens the texture. In the ISD method, the tilt of the template layers depends on the angle at which the ISD-MgO layer is deposited [2]. Because the YBCO c-axis takes on the tilt of the template in this structure (but not in all structures made by the ISD method), we were able to prepare YBCO films with different tilts by using templates that had been deposited at different angles.

In general, the O(4) mode is used to characterize the out-of-plane texture of YBCO films [3]; in the xx/yy scattering configuration, the intensity of this peak relative to that of the O(2+/3-) phonon is considered a measure of c-axis misalignment, or tilt. Unfortunately, microcrystallites with a-axis orientation

also contribute to the intensity of the O(4) phonon, so it is difficult to separate the contribution of c-axis tilted grains from that of a-axis oriented grains, especially when the film is deposited on a tilted substrate. Analyzing YBCO films on ISD-MgO templates with various tilts showed (Fig. 2) that the intensities of the O(2+/3+) mode (440-445 cm^{-1}) and the O(4) mode (≈500 cm^{-1}) both increased as the ISD deposition angle increased. But the intensity of the O(2+/3+) peak seemed to be affected only by the tilt of the substrate, unlike the O(4) peak, whose intensity varied across the film's surface as a result of variations in the local concentration of a-axis oriented grains.

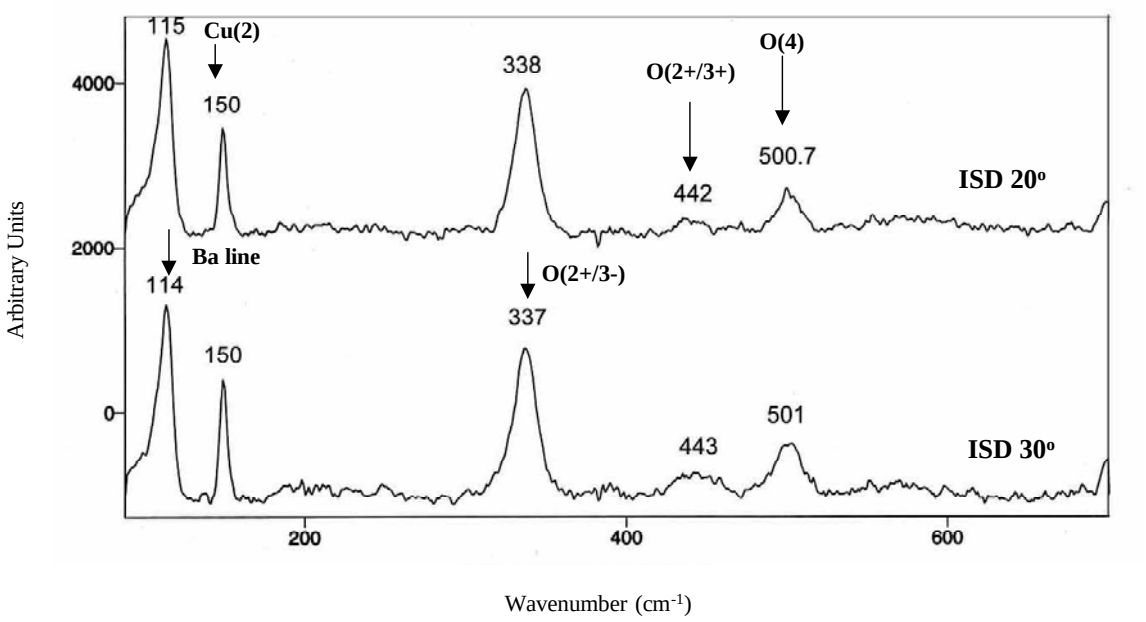

Fig. 2. Raman spectra of YBCO films on SRO-buffered ISD templates showing $I_{O(2+/3+)}$ increases as ISD deposition angle increases from 20° to 30°.

According to Iliev et al. [1], the O(2+/3+) mode is generated by in-phase bond bending of O(2) and O(3) atoms in CuO_2 planes. For orthorhombic YBCO, this peak appears when the YBCO film is tilted. Because the positions of the Cu(2) and O(4) peaks (at ≈150 and 500 cm^{-1}, respectively) indicated that the YBCO films of this study were fully oxygenated, we were also able to confirm that the O(2+/3+) peak was not generated by tetragonal domains, and that the only factor affecting its intensity was the tilt of the orthorhombic YBCO layer. Figure 3 plots the $I_{O(2+/3+)}/I_{O(2+/3-)}$ intensity ratio versus the deposition angle of the ISD-MgO layer, where $I_{O(2+/3+)}$ and $I_{O(2+/3-)}$ are the integrated intensities of the O(2+/3+) peak at ≈440 cm^{-1} and O(2+/3-) peak at ≈337 cm^{-1}, respectively.

Each point in the plot is the average of intensity ratios that were obtained from l Raman spectra recorded at four different spots. The intensity ratio was used, rather than $I_{O(2+/3+)}$, to normalize the results. $I_{O(2+/3-)}$ was used as the normalization factor, because it is less sensitive than other modes to changes in the film's oxygenation and composition. The figure shows that the $I_{O(2+/3+)}/I_{O(2+/3-)}$ ratio increases as the deposition angle increases. As a result, the intensity ratio can be used to directly measure the tilt of YBCO films on ISD templates.

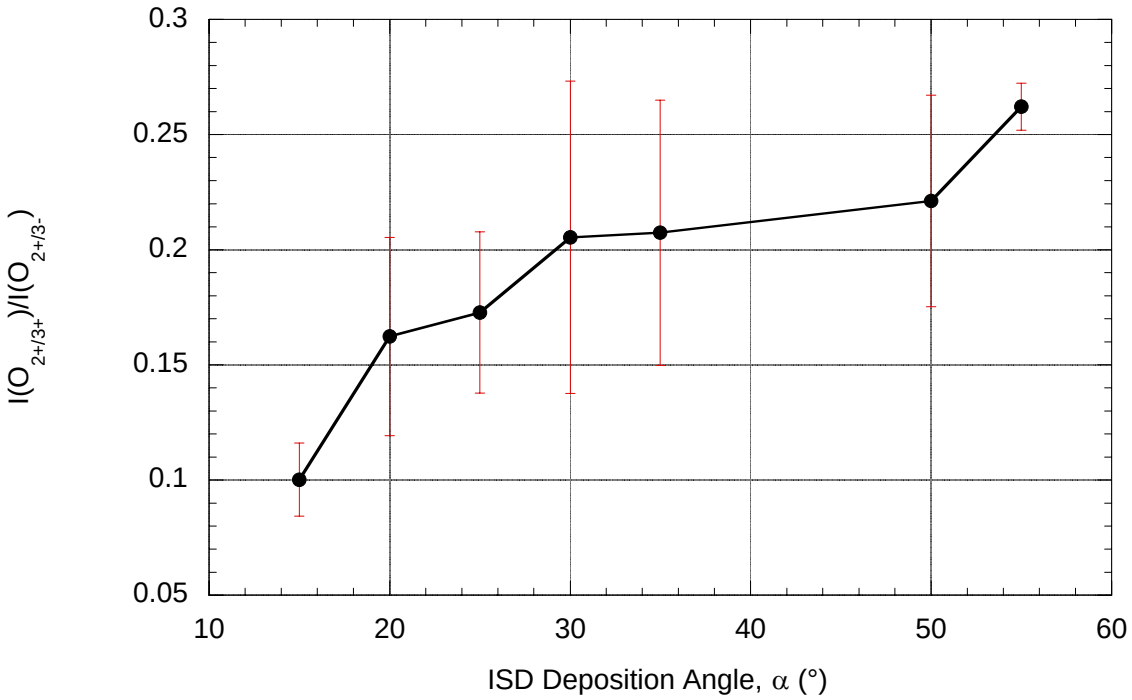

Fig. 3. Integrated ratio of $I_{O(2+/3+)}/I_{O(2+/3-)}$ as a function of the ISD angle for YBCO films deposited on various ISD angle SRO/M-ISD MgO/YSZ/HC templates.

YBCO Films on $SrRuO_3$ (SRO)-Buffered ISD-MgO Substrates

Samples made during the past several quarters have had the architecture YBCO/SRO/HE-MgO/ISD-MgO/YSZ/HC, in which a single SRO buffer layer replaces the CeO_2 and uppermost YSZ layer of the standard ISD architecture [4]. This structure will be abbreviated as YBCO/SRO/ISD in the remainder of this report. The ISD-MgO layer is deposited by electron beam evaporation (EBE) with the substrate at an inclination, α, as shown in Fig. 4. The value of α during deposition affects important characteristics of the ISD-MgO layer, e.g., its tilt (β),

which is defined in Fig. 5. Figures 6-8 show the effect of α on the surface roughness, tilt, and in-plane texture of ISD-MgO films. Until recently, the value of α was set at 55° during deposition of all ISD-MgO layers, because it appeared to give films with the sharpest texture and lowest surface roughness. However, ISD-MgO films made with α=35° have comparable surface roughness and in-plane texture, and their tilt is considerably smaller. To investigate the effect of tilt, we fabricated YBCO/SRO/ISD conductors using α of 35 and 55°, and compared their crystallographic and superconducting properties.

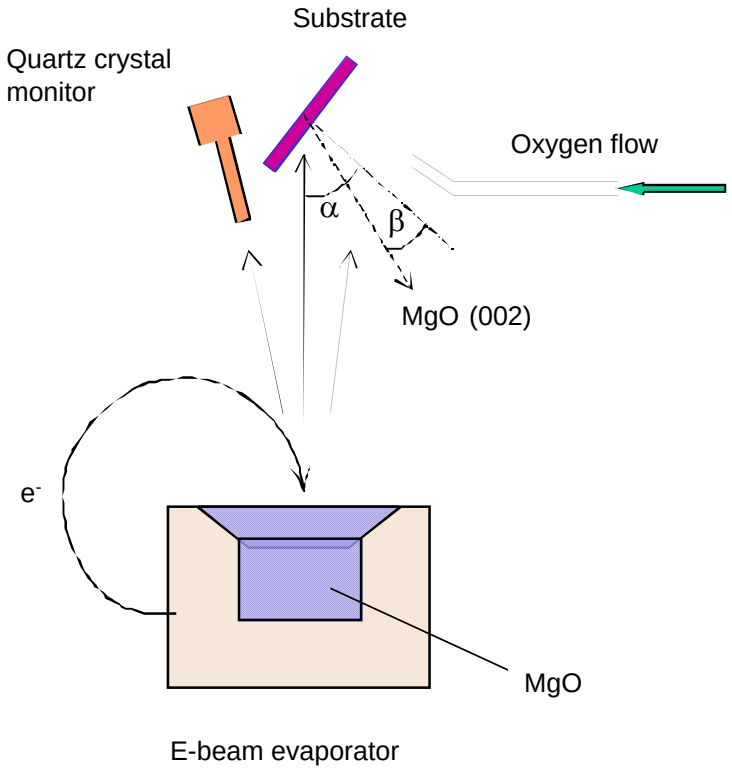

Fig. 4. Schematic illustrating the ISD deposition angle, α.

A 1-cm-wide ribbon of HC was polished to a mirror-finish by SuperPower, and then was cut into small (0.5 x 1.2 cm^2) coupons, which were mounted on a tiltable substrate stage using silver paste. Next, YSZ (thickness, 300 Å) was deposited on the coupons by electron beam evaporation (EBE). An ISD-MgO layer (thickness, 1 μm) was then deposited on the YSZ layer using EBE at room temperature and a deposition rate of 20 Å/s with α = 35°. On top of that layer was deposited an HE-MgO layer (thickness, 0.25 μm) using EBE with α = 0° at 700°C.

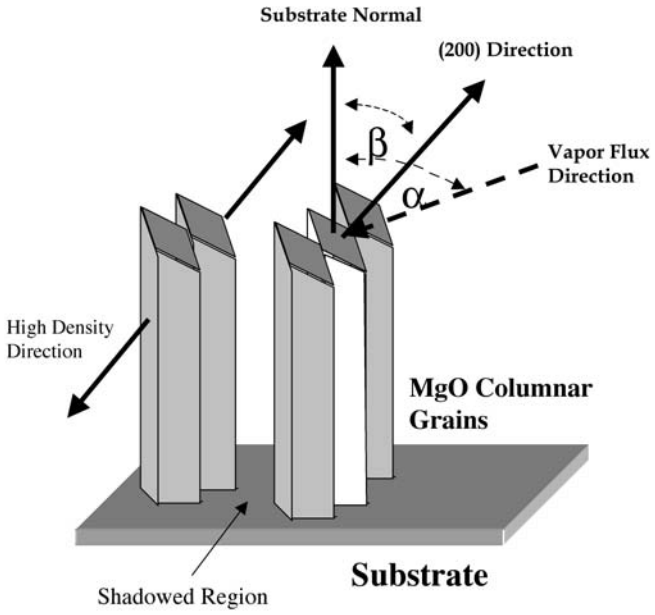

Fig. 5. Schematic illustrating tilt of ISD layer.

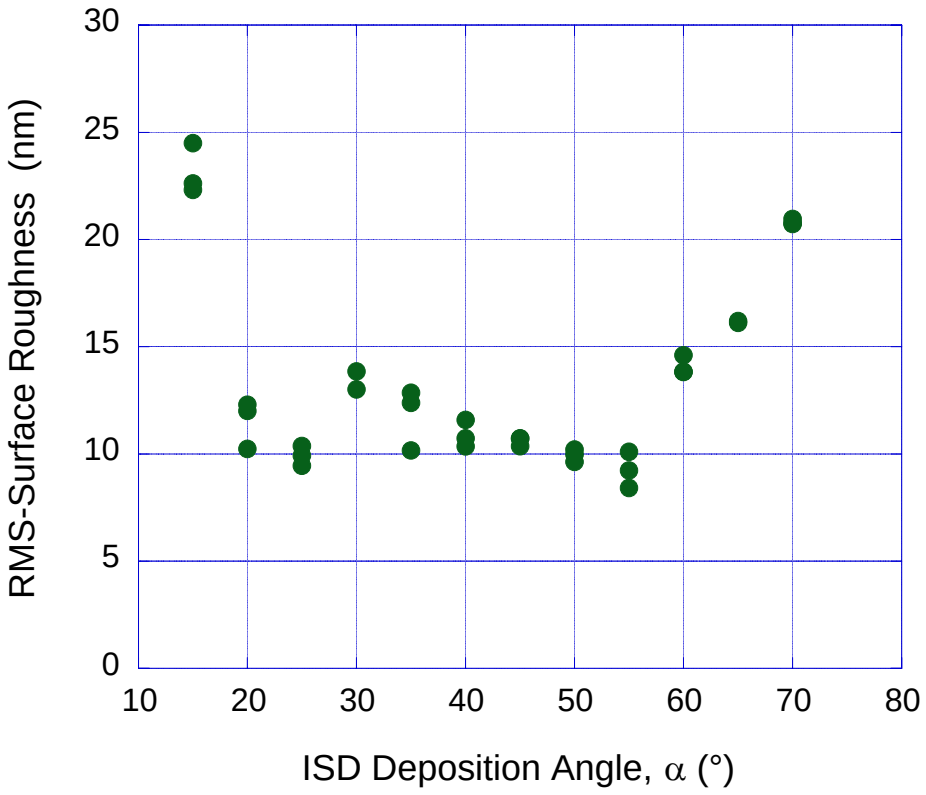

Fig. 6. Experimental data showing the relationship between ISD deposition angle, α, and surface roughness of ISD layer.

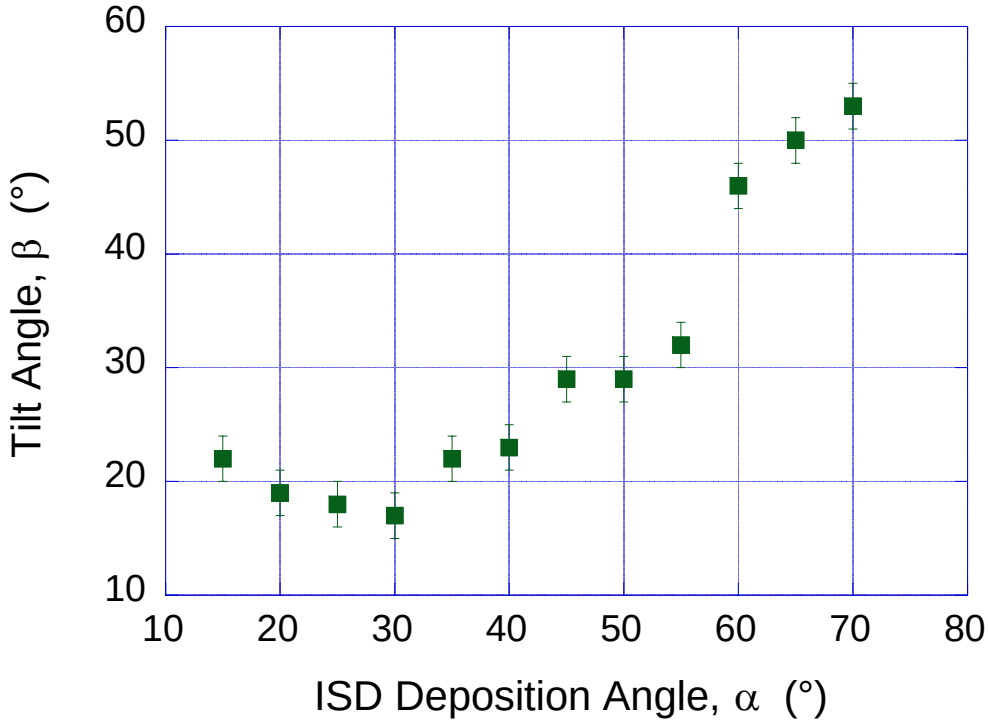

Fig. 7. Experimental data showing the relationship between ISD deposition angle, α, and tilt angle, β.

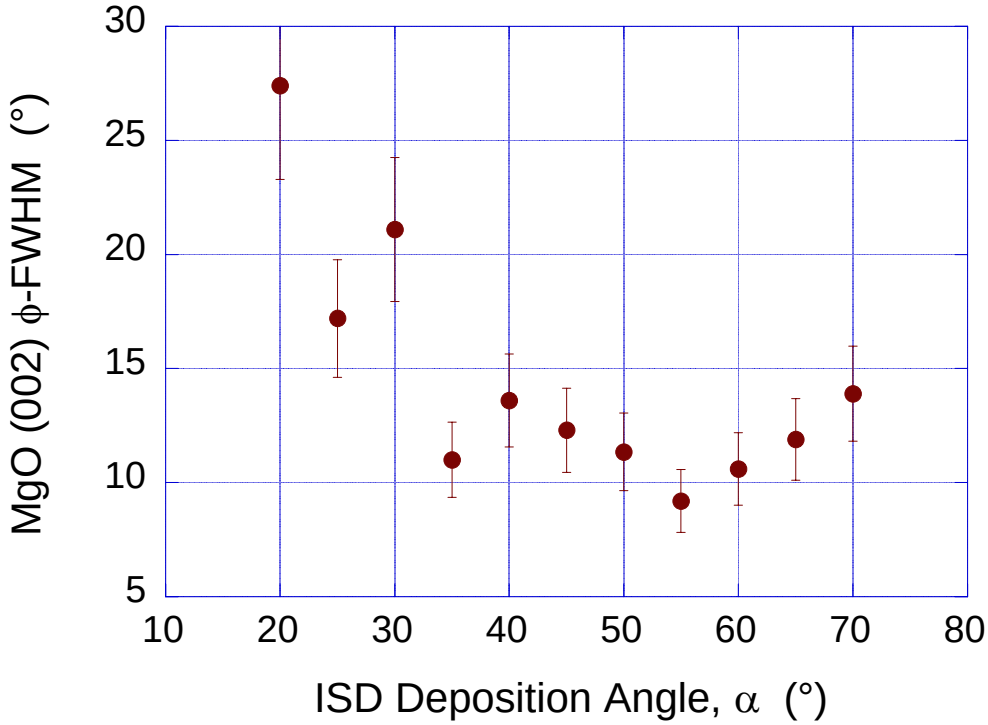

Fig. 8. Experimental data showing the relationship between ISD deposition angle, α, and in-plane texture of ISD layer.

ISD-MgO-coated metallic substrates were glued onto a heated stage using silver paste, and then SRO and YBCO films were deposited by pulsed laser deposition (PLD). A KrF excimer laser (Lambda Physik, Compex 201) with pulse duration of 25 ns and wavelength of 248 nm was focused onto the targets, which were rotated at 8 rpm. The YBCO and SRO targets (from Praxair Surface Technology) were 99.9 % pure and had a diameter of 2.54 cm and a thickness of 0.63 cm. The distance between the substrate and target was 6.5 cm. The SRO film was deposited at 770°C for 20 min in 50 mtorr of O_2 using a laser energy of 128 mJ/pulse and frequency of 4 Hz. YBCO was then deposited onto the SRO layer at 770°C in 240 mtorr of O_2 (deposition time, 30 min) using an energy of 140 mJ/pulse and frequency of 8 Hz. YBCO films were annealed for 90 min inside the PLD chamber at 450°C in 1 atm O_2.

YBCO(005) and SRO(020) X-ray ϕ-scans were used to evaluate the in-plane texture of YBCO and SRO, whereas a YBCO(007) ω-scan was used to examine the out-of-plane texture of YBCO. Figure 9 shows the YBCO(005), SRO(020), and MgO(002) pole figures of a representative YBCO/SRO/ISD sample made with α=35° and YBCO deposition time of 30 min.

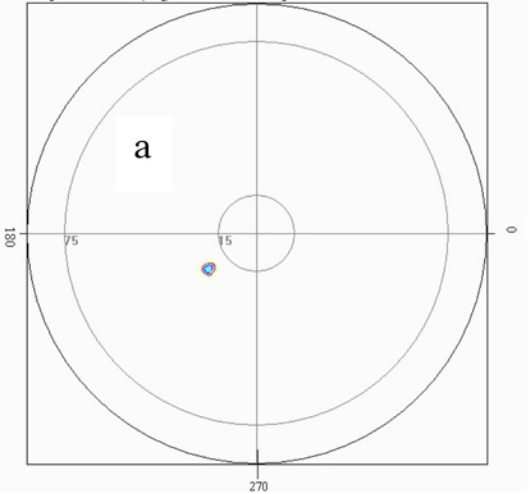
a
180
75
15
0
270

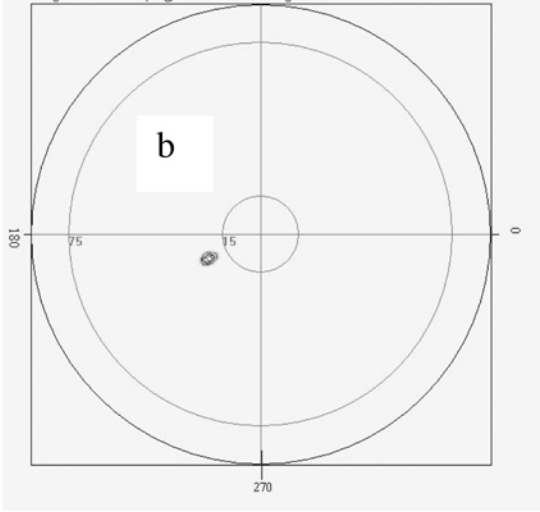
b
180
75
15
0
270

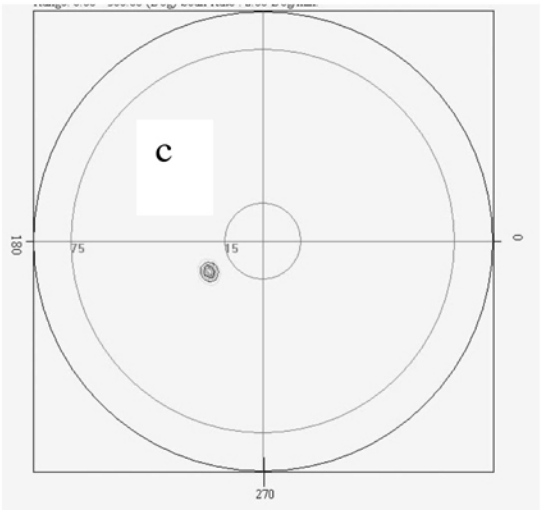
c
180
75
15
0
270

Fig. 9. Pole figures of a representative YBCO/SRO/ISD sample made with α=35° and YBCO deposition time of 30 min: a) YBCO(005), b SRO(020), and c) MgO(002).

From Fig. 9, we calculated a tilt of β=23° for the YBCO(005), SRO(020), and MgO(002) poles, which is smaller than the tilt (β=35°) for ISD layers with α=55°. The ϕ-scans (Fig. 10) indicated full width at half maximum (FWHM) values of 12.7° for MgO(002), 7.6° for SRO(020), and 7.6° for YBCO(005). The YBCO(007) ω-scan (Fig. 11) gave an FWHM of 2.8°. As the YBCO deposition time increased, the film texture improved. For example, another film, also made with α=35° but with a YBCO deposition time of 100 min, gave FWHM values of 12.9° for MgO(002), 6.2° for SRO(020), and 6.4° for YBCO(005), while the YBCO(007) ω-scan gave an FWHM of 2.4°.

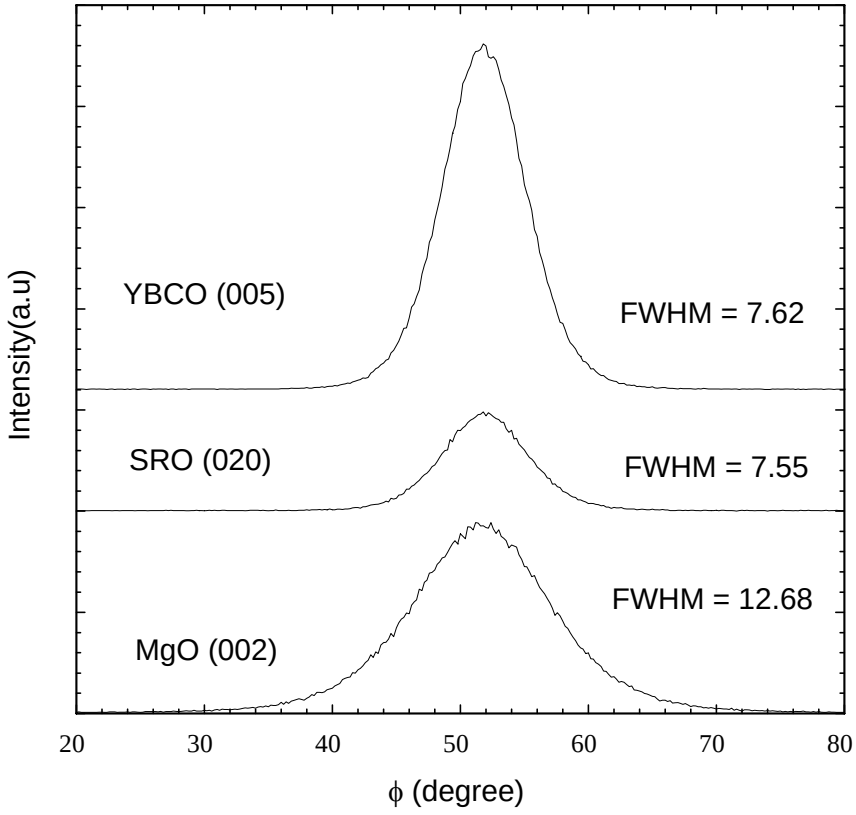

Fig. 10. The ϕ-scans of representative YBCO/SRO/ISD sample made with α=35° and YBCO deposition time of 30 min.

Templates with ISD layers deposited at α=35° had slightly poorer in-plane texture than templates whose ISD layers were deposited at α=55°. Eighteen samples whose ISD layers were deposited at α=35° gave an average FWHM of ≈13.3° for the MgO(002) pole, with the lowest value being 11.2°. Twelve samples

whose ISD layers were deposited at α=55° gave an average FWHM of 11.2°, with a best value of 10.5°. The in-plane texture of SRO and YBCO layers on MgO (α=35°) was also less sharp than that of SRO and YBCO on MgO (α=55°); however, the difference in texture was smaller. Samples made with a YBCO deposition time of 100 min, for example, had an average FWHM of 6.5° for the YBCO(005) pole of five samples whose ISD layers were deposited at α=35°; five samples made with α=55° had an average FWHM of 5.8° for the same pole. By contrast, there was little difference in the out-of-plane texture of YBCO. For a YBCO deposition time of 100 min, samples made with α=35° gave an average FWHM of 2.5°, whereas samples made with α=55° had an average FWHM of 2.6°.

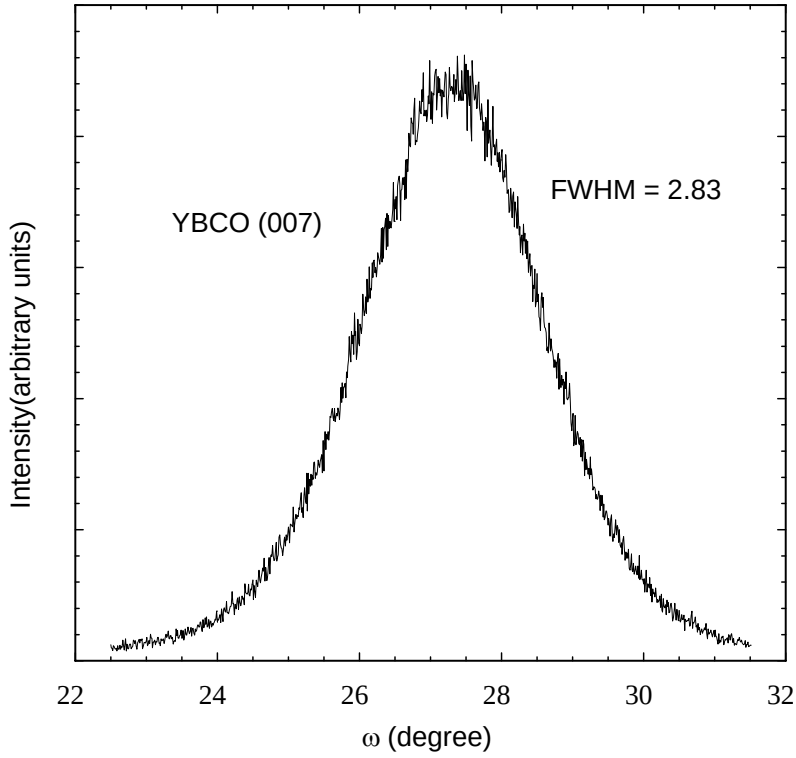

Fig. 11. YBCO(007) ω-scan for YBCO/SRO/ISD sample made with α=35° and YBCO deposition time of 30 min.

The T_c of YBCO was measured by an inductive method described elsewhere [2]. Figure 12 shows the inductive T_c of a YBCO/SRO/ISD sample whose YBCO layer was deposited at 770°C and whose ISD-MgO layer was deposited at α=35°. The film had an onset T_c of 89.8 K with a superconducting transition width (ΔT) of 1 K. The sharpness of the transition indicates that the film is homogeneous. The transport J_c of the YBCO films was measured by the four-probe contact

method. Results of the transport measurements (shown in Fig. 13) indicated that J_c=0.77x10^6 A/cm^2 for the sample (0.68 μm thick x 0.5 cm wide) at 77 K.

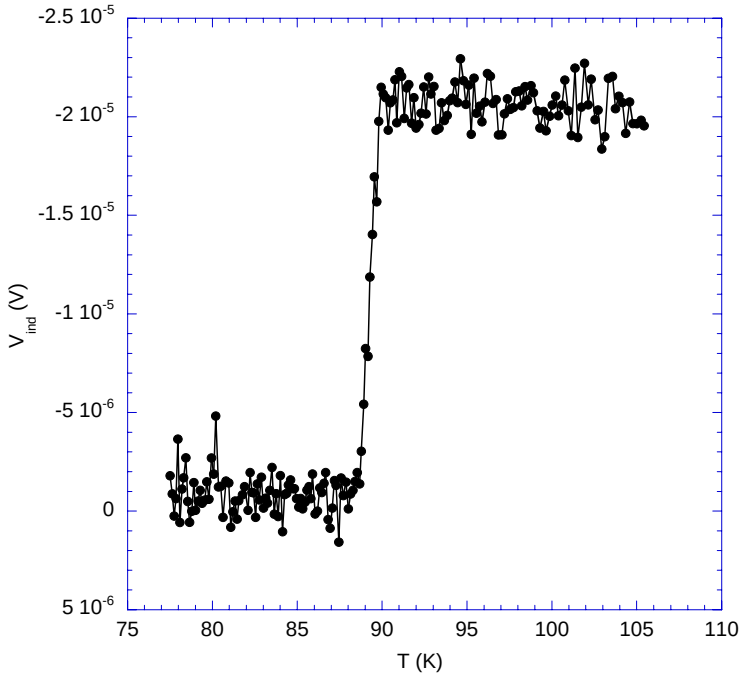

Fig. 12. Inductively measured superconducting transition of YBCO/SRO/ISD sample whose YBCO layer was deposited at 770°C and ISD-MgO layer was deposited at α=35°.

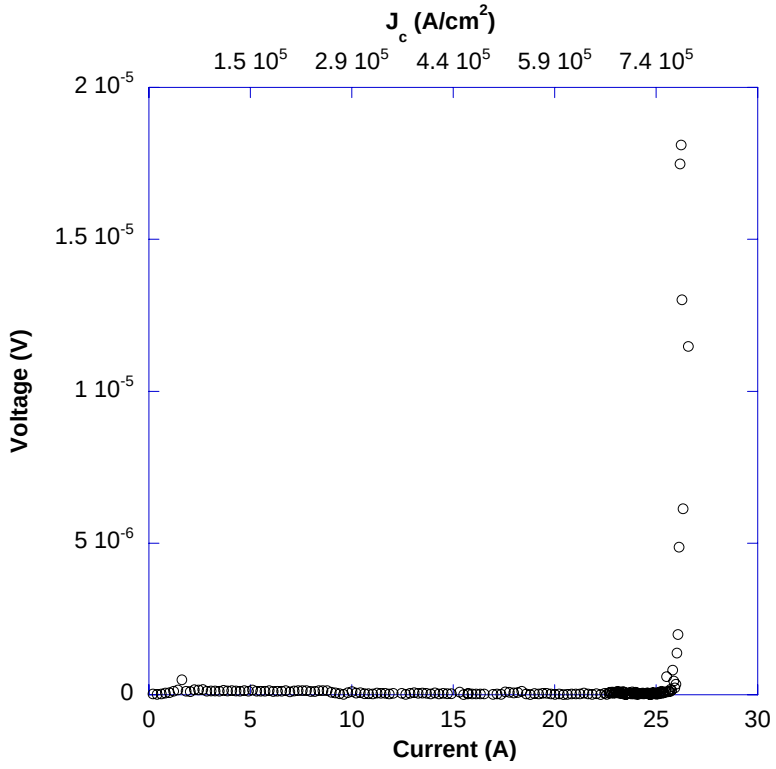

Fig. 13. Current-voltage curve for YBCO/SRO/ISD sample (0.68 μm thick x 0.5 cm wide) at 77 K. YBCO layer was deposited at 770°C and ISD-MgO layer was deposited at α=35°.

In summary, we compared the crystallographic and superconducting properties of YBCO/SRO/ISD conductors that were fabricated using ISD deposition angles of 35 and 55°. The in-plane texture of YBCO was sharp for samples made with either ISD deposition angle, although it was slightly sharper for samples whose ISD layers were deposited at α=55°. The out-of-plane texture of YBCO was also sharp, and was comparable for samples made with the two deposition angles. The most apparent difference between films made at the two deposition angles was in their tilt values, ≈23° for samples made at α=35° and ≈32° for samples made at α=55°. Despite their slightly poorer in-plane texture, samples made with α=35° consistently gave higher transport J_c. This finding suggests that the superconducting properties are influenced by the tilt of the YBCO films. To further investigate this possibility, we are studying the superconducting and crystalline properties of YBCO/SRO/ISD conductors made with α = 15, 20, 25, 30, 35, 40, 45, 50, and 55°.

References

1. M. N. Iliev, V. G. Hadjiev, and V. G. Ivanov, J. Raman Spectrosc. **27**, 333 (1996).

2. Argonne National Laboratory, Practical Superconductor Development for Electrical Power Applications, Annual Report for FY 2001.

3. N. Dieckmann, R. Kursten, M. Lohndorf, and A. Bock, Physica C **245**, 212 (1995).

4. Argonne National Laboratory, Practical Superconductor Development for Electrical Power Applications, Quarterly Report for Period Ending Sept. 30, 2003.

Interactions

Balu Balachandran discussed the HTSC program with DOE program managers on Feb. 3, 2004.

Balu Balachandran was invited to attend and give a talk at the ICMC Topical Meeting at University of Wollongong, Australia, Feb. 10-13, 2004.

Balu Balachandran attended the CCAS Board Meeting in Washington, D.C. on Feb. 25, 2004.

John Hull and Balu Balachandran visited S&C Electric Company, Evanston, IL on March 11, 2004 and held discussion on HTSC applications.

Publications and Presentations

Published/Submitted

B. Ma, M. Li, B. L. Fisher, R. E. Koritala, R. M. Baurceanu, S. E. Dorris, and U. Balachandran, Inclined-Substrate Pulsed Laser Deposition of Yttria-Stabilized Zirconia Template Film for YBCO Coated Conductors, Ceramic Transactions, 149 15-21 (2004).

K. Venkataraman, D. F. Lee, K. Leonard, L. Heatherly, S. Cook, M. Paranthaman, M. Mika, and V. A. Maroni, Reel-to-reel Diffraction and Raman Microscopy Analysis of Differentially Heat-Treated Y-BaF_2-Cu Precursor Films on Metre-Length RABiTS, Supercond. Sci. Tech., 17, 739-749 (2004).

K. Venkataraman, A. J. Kropf, C. U. Segre, Q. X. Jia, A. Goyal, B. W. Kang, S. Chattopadhyay, H. You, and V. A. Maroni, Detection of Interfacial Strain and Phase Separation in $MBa_2Cu_3O_{7-x}$ Thin Films using Raman Spectroscopy and X-Ray Diffraction Space Mapping, Physica C, 402, 1-16 (2004).

V. K. Vlasko-Vlasov, H. Claus, U. Welp, K. E. Gray, B. Ma, and U. Balachandran, Improving Ratio of the Grain Boundary and Bulk Critical Currents in $YBa_2Cu_3O_{7-\delta}$ Films, Appl. Phys. Lett., 84(2), 242-244 (2004).

B. Ma, R. E. Koritala, B. L. Fisher, K. K. Uprety, R. Baurceanu, S. E. Dorris, D. J. Miller, P. Berghuis, K. E. Gray, and U. Balachandran, High Critical Current Density of YBCO Coated Conductors Fabricated by Inclined Substrate Deposition, Physica C, 403, 183-190, (2004).

U. Balachandran, B. Ma, B. L. Fisher, R. E. Koritala, and D. E. Miller, Fabrication of YBCO-Coated Conductors by Inclined Substrate Deposition, Invited extended abstract presented at the 11th U.S.-Japan Workshop on High-T_c Superconductors, Kanagawa, Japan, Oct. 31-Nov. 2, 2003.

B. Ma, K. K. Uprety, B. L. Fisher, R. E. Koritala, S. E. Dorris, and U. Balachandran, YBCO-Coated Conductors Fabricated by Inclined Substrate Deposition Technique, Paper presented at the 2004 Intl. Cryogenic Matls. Conf. (ICMC 2004) Topic Workshop on Materials Processing, Microstructure and Critical Current of Superconductors, Wollongong, Australia, Feb. 10-13, 2004.

R. M. Baurceanu, S. E. Dorris, T. Wiencek, B. Ma, R. E. Koritala, V. A. Maroni, K. Venkataraman, M. Mika, and U. Balachandran, Optimum Copper Content of Silver for $YBa_2Cu_3O_{7-\delta}$ (YBCO) Coated Conductors, Submitted to Physica C (Feb. 2004).

K. K. Uprety, B. Ma, R. E. Koritala, R. M. Baurceanu, T. P. Weber, B. L. Fisher, S. E. Dorris, R. A. Erck, V. A. Maroni, and U. Balachandran, Growth of YBCO Film on $SrRuO_3$-buffered MgO Substrate, Submitted to Superconductor Science and Technology (Nov. 2003).

T. P. Weber, B. Ma, U. Balachandran, and M. McNallan, Fabrication of Biaxially-Textured Magnesium Oxide Thin Films by Ion-Beam-Assisted Deposition, Submitted to Thin Solid Films (March 2004).

Patents: 2000-2003

Fabrication of High Temperature Superconductors
Uthamalingam Balachandran, Stephen E. Dorris, Beihai Ma, and Meiya Li
U.S. Patent No. 6,579,360 (June 17, 2003).

Metallic Substrates for High-Temperature Superconductors
T. Truchan, D. Miller, K. C. Goretta, U. Balachandran, and R. Foley (U. of IL)
U.S. Patent No. 6,455,166 (Sept. 24, 2002).

Method for Preparing High-Temperature Superconductor
Uthamalingam Balachandran and Michael P. Chudzik
U.S. Patent No. 6,361,598 (March 26, 2002).

Shielded High-T_C BSCCO Tapes or Wires for High-Field Applications
Uthamalingam Balachandran, Milan Lelovic, and Nicholas G. Eror
U.S. Patent No. 6,252,096 (June 26, 2001); U.S. Patent 6,466,805 (Oct. 15, 2002).

Thermomechanical Means to Improve Critical Current Density of BSCCO Tapes
Uthamalingam Balachandran, Roger B. Poeppel, Pradeep Haldar (IGC), and Lesizek Motowidlo (IGC), U.S. Patent 6,240,619 (June 5, 2001).

Method of Manufacturing a High-Temperature Superconductor with Improved Transport Properties
Uthamalingam Balachandran, Richard Siegel, and Thomas Askew
U.S. Patent No. 6,191,075 (February 20, 2001).

Bearing Design for Flywheel Energy Storage Using High-T_c Superconductors
John R. Hull and Thomas M. Mulcahy
U.S. Patent No. 6,153,958 (Nov. 28, 2000).

Method and Apparatus for Measuring Gravitational Acceleration Utilizing a High- Temperature Superconducting Bearing
John R. Hull
U.S. Patent 6,079,267 (June 27, 2000).

Improvements in Levitation Pressure and Friction Losses in Superconducting Bearings,
John R. Hull
U.S. Patent 6,175,175 (January 16, 2001).

Trapped Field Internal Dipole Superconducting Motor/Generator
John R. Hull
U.S. Patent 6,169,352 (January 2, 2001).

Reluctance Apparatus for Flywheel Energy Storage
John R. Hull
U.S. Patent 6,097,118 (August 1, 2000).

Large Area Bulk Superconductors
Dean J. Miller and Michael B. Field
U.S. Patent 6,410,487 (June 25, 2002).